

### 3,6-Dioxypyridazine bridged tungsten–tungsten quadruple bonds. Comparisons of electron delocalisation with oxalate bridged compounds†‡

Malcolm H. Chisholm,<sup>\*a</sup> Robin J. H. Clark,<sup>\*b</sup> Christopher M. Hadad<sup>\*a</sup> and Nathan J. Patmore<sup>a</sup>

<sup>a</sup> Department of Chemistry, The Ohio State University, 100 W. 18th Avenue, Columbus, OH 43210-1173, USA. E-mail: chisholm@chemistry.ohio-state.edu

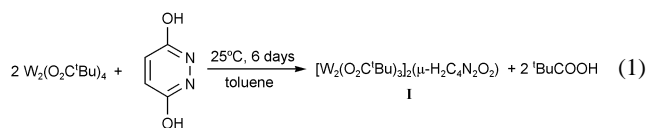
<sup>b</sup> Christopher Ingold Laboratories, University College London, 20 Gordon Street, London, UK WC1H 0AJ. E-mail: r.j.h.clark@ucl.ac.uk

Received (in West Lafayette, IN, USA) 10th September 2003, Accepted 28th October 2003

First published as an Advance Article on the web 20th November 2003

The preparation and characterisation of the tungsten–tungsten quadruply bonded, 3,6-dioxypyridazine bridged complex [(<sup>t</sup>BuCO<sub>2</sub>)<sub>3</sub>W<sub>2</sub>]<sub>2</sub>(μ-H<sub>2</sub>C<sub>4</sub>N<sub>2</sub>O<sub>2</sub>) and its single electron oxidised radical cation are reported and, when compared with related bridged dimolybdenum complexes, reveal a different mechanism of electronic coupling from that seen in related oxalate bridged systems.

We describe here our preparation and characterization of a 3,6-dioxypyridazine compound wherein two tungsten–tungsten quadruple bonds are electronically coupled. The electronic structure of this compound is particularly interesting with regard to recent studies reported by Cotton<sup>1</sup> and earlier work in this laboratory.<sup>2–4</sup>



Compound **I**, [(<sup>t</sup>BuCO<sub>2</sub>)<sub>3</sub>W<sub>2</sub>]<sub>2</sub>(μ-H<sub>2</sub>C<sub>4</sub>N<sub>2</sub>O<sub>2</sub>), is isolated as a purple microcrystalline air-sensitive material, as outlined in eqn. (1). It forms needles from hydrocarbon solutions of a size too small for conventional single-crystal X-ray diffraction studies. Most likely in the solid state, it exists as a coordination polymer by way of weak intermolecular W⋯O interactions.<sup>5</sup> This matter is currently under further investigation. The solution characterization data, however, leave little doubt as to the molecular nature of this compound, which is discussed next.

In order to aid in the interpretation of some of the electrochemical properties and spectroscopic data, *vide infra*, we carried out electronic structure calculations on the model formate bridged compound [(HCO<sub>2</sub>)<sub>3</sub>W<sub>2</sub>]<sub>2</sub>(μ-H<sub>2</sub>C<sub>4</sub>N<sub>2</sub>O<sub>2</sub>) in C<sub>2</sub> symmetry employing density functional theory with the aid of the Gaussian 98 suite of programs.<sup>6</sup> A vibrational frequency analysis verified the structure to be a local minimum on the potential energy surface (not the case in C<sub>2v</sub> symmetry). The calculated molecular structure is shown in Fig. 1 and selected bond distances and angles are given in Table 1. The frontier molecular orbitals and their energies are given in Fig. 2. The HOMO and HOMO-1 are in-phase and out-of-phase combinations of M<sub>2</sub> δ orbitals and the degree of M<sub>2</sub>⋯M<sub>2</sub> coupling can be gleaned from the energy separation of these two orbitals, 0.34 eV. A further indication of the strong electronic coupling is seen in the energy separations between the in- and out-of-phase combinations of the four π and two M<sub>2</sub> σ-orbitals. Indeed, the in-phase M<sub>2</sub> σ combination shows significant M<sub>2</sub>⋯M<sub>2</sub> bonding even at a distance of 3.6 Å. The LUMO is a ligand bridge π\* orbital and very close in energy is the LUMO+1 which in terms of M<sub>4</sub> σ

orbitals is σ<sub>3</sub>, being M<sub>2</sub> antibonding and M<sub>2</sub>⋯M<sub>2</sub> bonding (see Fig. 2).

Compound **I** shows intense absorptions in the visible region of the electronic spectrum and its purple colour in tetrahydrofuran derives from λ<sub>max</sub> = 704 nm (1.76 eV), ε ~ 8900 M<sup>-1</sup> cm<sup>-1</sup>. Based on the electronic structure calculation, this can reasonably be assigned to the HOMO → LUMO transition which is a fully-allowed MLCT transition. Time-dependent density functional theory (TDDFT) calculations confirm this and predict this transition to be at 561 nm (2.21 eV). Whilst there is not an unreasonable difference in energy between the calculated and observed spectrum (*ca.* 0.5 eV), we have noted before that TDDFT calculations ignore spin-orbit coupling and consistently overestimate the energy of W<sub>2</sub> δ to bridge π\* transitions in dicarboxylate linked W<sub>4</sub>-containing compounds.<sup>5</sup>

With excitation at 633 nm, compound **I** shows certain pronounced resonance-enhanced bands together with overtones and combination bands in the Raman spectrum. By comparison with the Raman spectrum calculated for the model compound [(HCO<sub>2</sub>)<sub>3</sub>W<sub>2</sub>]<sub>2</sub>(μ-H<sub>2</sub>C<sub>4</sub>N<sub>2</sub>O<sub>2</sub>), we assign these as shown in Table 2. Representations of these vibrational modes are given at <http://www.chemistry.ohio-state.edu/~chisholm/movies.html>. The resonance-enhancement of these bands is consistent with excitation from the W<sub>4</sub> δ HOMO to bridge π\* LUMO.

In tetrahydrofuran, compound **I** shows two oxidation waves by cyclic voltammetry, CV. The first is reversible and the second

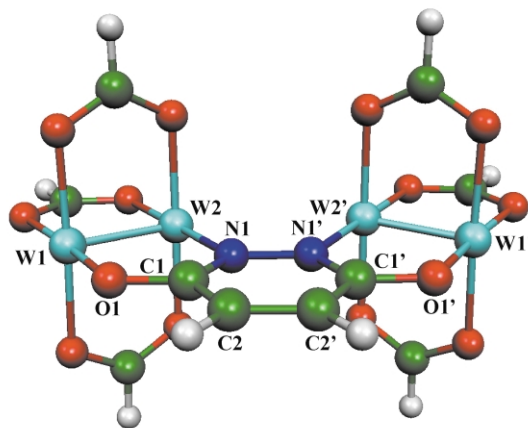


**Fig. 1** View of the structure of [(HCO<sub>2</sub>)<sub>3</sub>W<sub>2</sub>]<sub>2</sub>(μ-N<sub>2</sub>C<sub>4</sub>O<sub>2</sub>H<sub>2</sub>) calculated in C<sub>2</sub> symmetry. Atom labels in parentheses are related by the C<sub>2</sub> axis.

**Table 1** Selected bond lengths (Å), angles (°), and torsional angles (°) calculated for [(HCO<sub>2</sub>)<sub>3</sub>W<sub>2</sub>]<sub>2</sub>(μ-H<sub>2</sub>C<sub>4</sub>N<sub>2</sub>O<sub>2</sub>)

W1–W2	2.206	W2–N1	2.131	N1–N1'	1.391
W2–W2'	3.596	O1–C1	1.305	C1–C2	1.421
W1–O1	2.050	C1–N1	1.366	C2–C2'	1.365
		W1–O1–C1	120.59	W2–N1–N1'	121.54
		W2–N1–C1	119.05	O1–C1–N1	118.03
		W2–N2–N2'–W2'	2.17	W1–W2–W2'–W1'	7.97

† Electronic Supplementary Information (ESI) available: details of instrumentation; experimental procedures; frontier molecular orbital diagrams for [(HCO<sub>2</sub>)<sub>3</sub>Mo<sub>2</sub>]<sub>2</sub>(μ-H<sub>2</sub>C<sub>4</sub>N<sub>2</sub>O<sub>2</sub>); electrochemical data and Raman spectrum of **I**. See <http://www.rsc.org/suppdata/cc/b3/b310982h/>

‡ Dedicated to Professor C. S. Parmenter on the occasion of his 70th birthday.

quasi-reversible. These two waves are well separated. By CV and pulsed differential voltammetry, PDV, the separation between these waves,  $E_{1/2}^2 - E_{1/2}^1 = 630$  mV. This gives a calculated  $K_C$  value of  $4.5 \times 10^{10}$  which reliably establishes the single electron oxidised form of the compound as Class III in the Robin Day scheme;<sup>8</sup> in other words the oxidised mixed-valence cation is fully delocalised. Consistent with this, the EPR spectrum of  $\text{I}^+\text{PF}_6^-$  at 250 K (see Fig. 3), formed in the reaction between **I** and  $\text{Cp}_2\text{Fe}^+\text{PF}_6^-$  in 2-Me-THF, shows  $g = 1.801$  and  $A_{\text{av}} = 27$  Gauss, characteristic of the unpaired electron being in a molecular orbital that is fully delocalised over the four tungsten nuclei:  $^{183}\text{W}$ ,  $I = \frac{1}{2}$ , 14.5% natural abundance.<sup>9</sup> Furthermore, the electronic absorption spectrum of  $\text{I}^+\text{PF}_6^-$  in THF, displayed in Fig. 4, shows a low energy absorption band centred at 2650 nm,  $\epsilon \sim 5000 \text{ M}^{-1} \text{ cm}^{-1}$ , in addition to a sharper band at 811 nm,  $\epsilon \sim 14,000 \text{ M}^{-1} \text{ cm}^{-1}$ . While the latter can be assigned to the single electron transition from the HOMO to the LUMO (or maybe a LMCT), the band in the infrared region is a direct measure of the coupling,  $2H_{\text{AB}}$ .<sup>10</sup>

The strongly coupled  $\text{W}_2$  centers in **I** are in agreement with the recent report by Cotton *et al.* for cyclic polyamidato-linked  $\text{Mo}_2^{4+}$  centres supported by  $N,N'$ -di-*p*-anisylformamidinate ligands,  $[(\text{DAniF})_3\text{Mo}_2]_2(\text{bridge})$ .<sup>1</sup> The strongest coupling was seen in the order of the bridges  $\text{A} < \text{B} < \text{C}$  shown in Scheme 1, and the authors noted that in all cases the values of  $K_C$  were larger than that seen for oxalate, **D**, despite the geometrical equivalence of the ligands in separating the two  $\text{M}_2$  centers.

It had been noted previously that when the 3,6-dioxypyridazine bridge united two  $[\text{Mo}_2(\text{O}_2\text{C}^t\text{Bu})_3]^+$  units in the molybdenum analogue of **I**,<sup>3</sup> the  $K_C$  value determined by CV,  $1.7 \times 10^7$ , was greater than  $K_C = 5.4 \times 10^4$  obtained under otherwise identical conditions for the oxalate-bridged compound,  $[(^t\text{BuCO}_2)_3\text{Mo}_2]_2(\mu-$

$\text{O}_2\text{CCO}_2)$ .<sup>2</sup> It is then at first seemingly surprising that the  $K_C$  value for  $[(^t\text{BuCO}_2)_3\text{W}_2]_2(\mu-\text{O}_2\text{CCO}_2)$  is larger,  $1.3 \times 10^{12}$ , than that reported herein for **I**,  $4.5 \times 10^{10}$ .

**Table 2** Comparison of the experimental resonance Raman band wavenumbers of  $[(^t\text{BuCO}_2)_3\text{W}_2]_2(\mu-\text{H}_2\text{C}_4\text{N}_2\text{O}_2)$  with the calculated values for  $[(\text{HCO}_2)_3\text{W}_2]_2(\mu-\text{H}_2\text{C}_4\text{N}_2\text{O}_2)$ , and the band assignments

Experimental $\nu/\text{cm}^{-1}$	Calculated $\nu/\text{cm}^{-1}$	Assignment
308	337	$\text{W}_4$ symmetric stretch
616	633	W–O(bridge) symmetric stretch
871	882	W–W stretch and bridge “breathing”
1273	1313	Symmetric bridge ring stretch
1566	1624	Symmetric bridge ring stretch

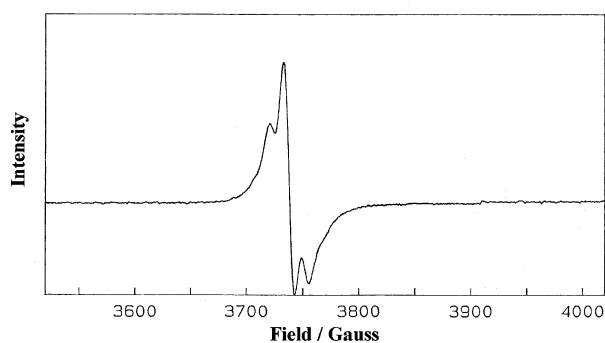


**Fig. 3** EPR spectrum of  $\text{I}^+\text{PF}_6^-$  at 250 K in 2-Me-THF.

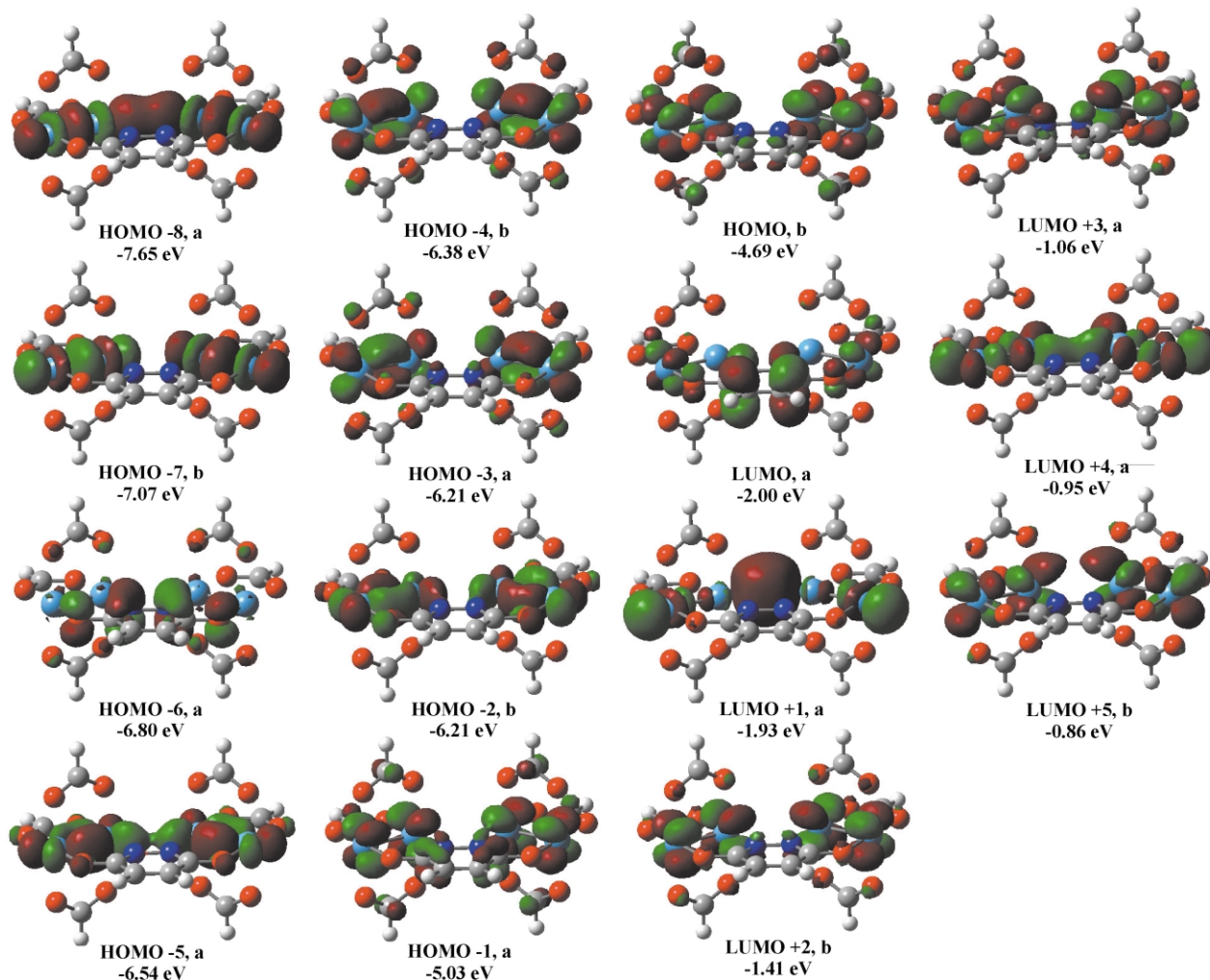


**Fig. 2** Frontier molecular orbital plots calculated for  $[(\text{HCO}_2)_3\text{W}_2]_2(\mu-\text{N}_2\text{C}_4\text{O}_2\text{H}_2)$ . Orbitals are drawn at an isosurface value of 0.04.

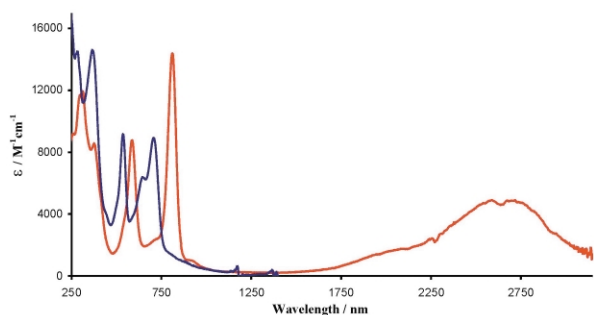
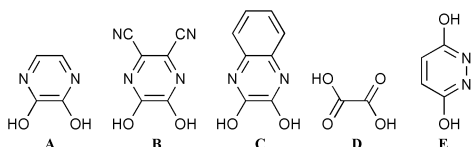


**Fig. 4** UV/Vis/NIR spectra of **I** (blue trace) and  $\text{I}^+\text{PF}_6^-$  (red trace) in THF.



**Scheme 1** Examples of ligands used to bridge  $\text{M}_2$  centres. The amidato ligands are drawn in the hydroxyamine tautomeric form.

The degree of electronic coupling between  $\text{M}_2$  centers united by a bridging ligand scales with distance between the  $\text{M}_2$  centers and correlates with the interactions between the  $\text{M}_2$  frontier orbitals, principally  $\text{M}_2 \delta$ , and the bridge  $\pi$  and  $\pi^*$  orbitals. The oxalate bridge, **D**, in contrast to the other cyclic polyamidato bridges **A**, **B**, **C** and **E**, has filled  $\pi$ -orbitals that lie considerably lower in energy than those of the  $\text{M}_2 \sigma$ ,  $\pi$  and  $\delta$  combinations. For the cyclic polyamidates the highest occupied bridge  $\pi$  orbitals are within this

range. For the specific case at hand, the HOMO-6 at  $-6.80$  eV is a bridge-centered MO, while in the case of the molybdenum analogue  $[(\text{HCO}_2)_3\text{Mo}_2]_2(\mu\text{-H}_2\text{C}_4\text{N}_2\text{O}_2)$ , this orbital is the HOMO-2 at  $-6.71$  eV, roughly 1 eV below the  $\delta$  combinations, the HOMO and HOMO-1 which are at  $-5.25$  eV and  $-5.50$  eV, respectively. Thus, aside from the obvious differences between the electronic structures of these  $\text{M}_4$  complexes involving the bridges derived from deprotonation of **D** and **E** that arise from the geometrical arrangement of the  $\text{M}_2$  units, the electronic communication in their radical cations differ substantially. In the case of the oxalate bridges, the electron delocalization principally arises from  $\text{M}_2 \delta$  coupling with the LUMO of the ligand bridge and this readily accounts for the much larger  $K_C$  value,  $1.3 \times 10^{12}$ , seen for  $[(\text{tBuCO}_2)_3\text{W}_2]_2(\mu\text{-O}_2\text{CCO}_2)$  relative to its molybdenum counterpart,  $5.4 \times 10^4$ . In the case of the 3,6-dioxypyridazine bridge, and by inference the related cyclic diamidate ligands studied by Cotton and coworkers,<sup>1</sup> the higher energy of the bridge  $\pi$  MOs assists in electron delocalization in the radical cations by a ‘hole hopping’ mechanism. Given that the highest energy bridge  $\pi$  MO is closer to the HOMO in the case of the  $\text{Mo}_4$  complex, the hole hopping contribution to the stability of the radical cations will be more important for molybdenum than for tungsten. These differences are depicted diagrammatically in Fig. 5 for the two bridging ligands. For closely related compounds the energy of the  $\text{W}_2 \delta$  orbital lies *ca.* 0.5 eV higher than that of its  $\text{Mo}_2 \delta$  counterpart. This proposed explanation for the relative ordering of the  $K_C$  values lends itself to experimental testing and further studies are planned.

We thank the National Science Foundation for support of this work. The Ohio Supercomputer Center is gratefully acknowledged for computational resources with which the DFT calculations were performed.

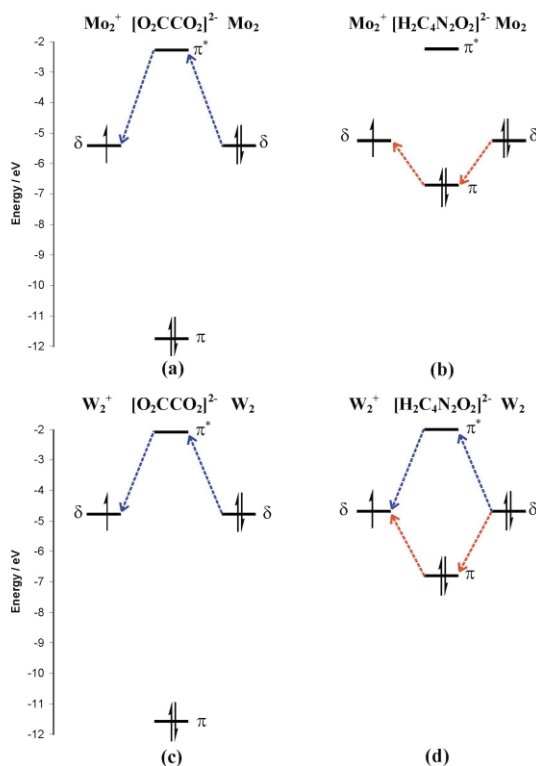


**Fig. 5** Frontier MO energy level diagram depicting the relative energies of the  $\text{M}_2 \delta$  (HOMO) ( $\text{M} = \text{Mo}, \text{W}$ ) and the bridging ligand filled and empty  $\pi$  orbitals for oxalate and 3,6-dioxypyridazine, based upon calculations on the neutral formate model compounds. The dotted arrow represents the energetically favoured mechanism of electron delocalization *via* ‘electron hopping’ (in blue) or ‘hole hopping’ (in red).

## Notes and references

- 1 F. A. Cotton, J. P. Donahue, C. A. Murillo, L. M. Perez and R. Yu, *J. Am. Chem. Soc.*, 2003, **125**, 8900.
- 2 R. H. Cayton, M. H. Chisholm, J. C. Huffman and E. B. Lobkovsky, *J. Am. Chem. Soc.*, 1991, **113**, 8709.
- 3 R. H. Cayton, M. H. Chisholm, E. F. Putilina and K. Foltling, *Polyhedron*, 1993, **12**, 2627.
- 4 R. H. Cayton, M. H. Chisholm, J. C. Huffman and E. B. Lobkovsky, *Angew. Chem., Int. Ed. Engl.*, 1991, **30**, 862.
- 5 B. E. Bursten, M. H. Chisholm, R. J. H. Clark, S. Firth, C. M. Hadad, A. M. MacIntosh, P. J. Wilson, P. M. Woodward and J. M. Zaleski, *J. Am. Chem. Soc.*, 2002, **124**, 3050; B. E. Bursten, M. H. Chisholm, R. J. H. Clark, S. Firth, C. M. Hadad, P. J. Wilson, P. M. Woodward and J. M. Zaleski, *J. Am. Chem. Soc.*, 2002, **124**, 12244.
- 6 *Gaussian 98*, Revision A9, M. J. Frisch, G. W. Trucks, H. B. Schlegel, G. E. Scuseria, M. A. Robb, J. R. Cheeseman, J. A. Montgomery, T. V. Jr., K. N. Kudin, J. C. Burant, J. M. Millam, S. S. Iyengar, J. Tomasi, V. Barone, B. Mennucci, M. Cossi, G. Scalmani, N. Rega, G. A. Petersson, H. Nakatsuji, M. Hada, M. Ehara, K. Toyota, R. Fukuda, J. Hasegawa, M. Ishida, T. Nakajima, Y. Honda, O. Kitao, H. Nakai, M. Klene, X. Li, J. E. Knox, H. P. Hratchian, J. B. Cross, C. Adamo, J. Jaramillo, R. Gomperts, R. E. Stratmann, O. Yazyev, A. J. Austin, R. Cammi, C. Pomelli, J. W. Ochterski, P. Y. Ayala, K. Morokuma, G. A. Voth, P. Salvador, J. J. Dannenberg, V. G. Zakrzewski, S. Dapprich, A. D. Daniels, M. C. Strain, O. Farkas, D. K. Malick, A. D. Rabuck, K. Raghavachari, J. B. Foresman, J. V. Ortiz, Q. Cui, A. G. Baboul, S. Clifford, J. Cioslowski, B. B. Stefanov, G. Liu, A. Liashenko, P. Piskorz, I. Komaromi, R. L. Martin, D. J. Fox, T. Keith, M. A. Al-Laham, C. Y. Peng, A. Nanayakkara, M. Challacombe, P. M. W. Gill, B. Johnson, W. Chen, M. W. Wong, C. Gonzalez and J. A. Pople, Gaussian, Inc., Pittsburgh, PA, 1998.
- 7 D. E. Richardson and H. Taube, *Inorg. Chem.*, 1981, **20**, 1278.
- 8 M. B. Robin and P. Day, *Adv. Inorg. Radiochem.*, 1967, **10**, 247.
- 9 M. H. Chisholm, B. D. Pate, P. J. Wilson and J. M. Zaleski, *Chem. Commun.*, 2002, 1084.
- 10 C. Creutz, *Prog. Inorg. Chem.*, 1983, **30**, 1; S. F. Nelson, *Chem. Eur. J.*, 2001, **6**, 581.